JOURNAL OF EXPERIMENTAL ZOOLOGY 290:652–661 (2001)

Covariance of Ion Flux Measurements Allows New Interpretation of *Xenopus laevis* Oocyte Physiology

ELLEN E. FASZEWSKI* AND JOSEPH G. KUNKEL
Department of Biology, University of Massachusetts, Amherst, Massachusetts 01003-5810

ABSTRACT An animal-vegetal net ionic current identified previously using voltage probe techniques in maturing *Xenopus laevis* oocytes has now been investigated using noninvasive ion-selective microelectrodes. Three-dimensional fluxes of hydrogen (H^+), potassium (K^+), and bicarbonate (HCO_3^-) were characterized with respect to the developmental stage and hemisphere of the oocyte and presence of surrounding follicular tissue. Variable effluxes of H^+ and HCO_3^- were recorded from both the animal and vegetal hemispheres. Variable influxes and effluxes of K^+ were also observed. The equatorial region, silent by voltage probe, exhibited fluxes of H^+ and K^+. Simultaneous measurement of pairs of ions allowed correlation analysis of two ion types. Notably for H^+ and K^+ data, positive and negative correlation at animal and vegetal poles respectively offer an explanation of the unpredictable results obtained when individual ions were observed independently. *J. Exp. Zool. 290:652–661, 2001.*

Previous electrophysiological studies have suggested that ionic currents are important in developmental events such as early polarity determination in the brown alga, *Fucus serratus* (Jaffe, '66) and in the South African clawed toad, *Xenopus* (Robinson, '79). The *Xenopus* research demonstrated the presence of a net positive current entering the animal pole and leaving the vegetal pole (Robinson, '79). This theory has been strengthened by subsequent studies where asymmetric currents were seen to travel along the dorso-ventral (Kunkel, '86; Bowdan and Kunkel, '90) and anterio-posterior (Overall and Jaffe, '85) axes in panoistic and merosistic insect follicles, respectively. In *Xenopus*, the main carrier of this positive inward current was explained to be an efflux of chloride that is calcium-dependent (Miledi, '82; Barish, '83). These past results in *Xenopus*, however, were obtained with noninvasive techniques (voltage probe) and invasive techniques (voltage clamping), which measure changes in net ionic current. The ion composition and any variability of the current had to be inferred by the addition of agonists/inhibitors to the extracellular media. As a result, many questions remain unanswered such as which ions contribute to the natural asymmetric fluxes in the absence of agonists/antagonists, where and in which direction do they travel, and, ultimately, what is the role of ion flux in early development.

As the ideas and concepts regarding the importance of ion fluxes in growth and development have progressed, so have the techniques with which these studies are carried out. The development of ion-selective electrodes by Jaffe and Levy ('87) has provided the ability to noninvasively collect ion flux data over extended periods of time (benefits of these ion-selective microelectrodes reviewed by Smith et al., '94). Use of these microelectrodes in this research has helped identify some of the specific ions that comprise the net current previously reported from developing *Xenopus* oocytes.

The aim of this study was to determine if proton (H^+), potassium (K^+), and bicarbonate (HCO_3^-) ions contribute to the observed asymmetrical current initially described by Robinson ('79) and to provide additional insight into the roles of these ions in early development. In addition, with the use of a multiple-ion head, allowing simultaneous data collection of two ion types, we sought to determine if there was meaningful correlation between ionic fluxes that possibly explains previously observed variability. These fluxes were then experimentally manipulated to study the underlying mechanisms. Defolliculation procedures were used to study the cellular origin of the flux and any possible interactions between the oocyte and its surrounding follicular tissue. Specific inhibi-

*Correspondence to: Ellen E. Faszewski, Department of Math/Natural Science, Wheelock College, 200 The Riverway, Boston, MA 02215. E-mail: efaszewski@wheelock.edu
Received 11 August 1999; Accepted 10 May 2001

tors were also utilized to examine the possible involvement of pump ATPases in the transport of specific ions (H^+ and K^+). Ortho-vanadate (Forgac et al., '83) and N-ethyl maleimide (Dröse and Altendorf, '97), known to inhibit P and V-type pumps, respectively, were used in this study. The combination of naturally occurring fluxes in conjunction with experimental manipulation allowed for further characterization of the asymmetrical current in *Xenopus* oocytes.

MATERIALS AND METHODS

Animals

Xenopus laevis adult females, obtained from Xenopus I (Ann Arbor, MI), were maintained at a constant temperature (30°C) on an 18/6 hour light/dark cycle. Glass aquaria, containing one gallon of spring water per frog, were placed in a low traffic area and cleaned as needed. Animals were fed beef liver twice a week (as much as they could consume in ten minutes), as suggested by Etheridge and Richter ('78).

Oocyte retrieval

Immediately prior to electrophysiology, females were anesthetized by chilling in an ice bath until immobile. The frog was then kept on ice during dissection in which oocytes were removed by partial ovariectomy and placed into normal Holtfreter's solution: 59.93 mM NaCl, 0.67 mM KCl, 0.68 mM $CaCl_2{\cdot}2H_20$, 2.38 mM $NaHCO_3$, pH = 7.8 (Rugh, '62). The female was then placed in an isolated chamber at room temperature and monitored during recovery.

Oocyte preparation

Oocytes were individually dissected out from the removed ovarian lobe in normal Holtfreter's with watchmaker forceps. Only oocytes in stages V and VI (Dumont, '72) were utilized. These stages, based on oocyte diameter, were further classified in H^+ experiments as V (1000–1100 μm), V+ (1100–1200 μm), VI (1200–1300 μm), and VI+ (1300–1400 μm). Oocytes that had been "plucked" from the ovarian lobe in this manner, referred to as "follicle-enclosed oocytes" (FEO), are immediately surrounded by a layer of follicle cells followed by an inner epithelial sheet of tissue.

Further manipulation of these FEOs could be performed by removal of these outer layers by manual defolliculation as described by Miledi and Woodward ('89).

Scanning electron microscopy

The defolliculation technique (removal of all follicular tissue including follicle cells) was monitored with scanning electron microscopy using a protocol adapted from Miledi and Woodward ('89). Oocytes were fixed in glutaraldehyde (2.5% in Holtfreter's solution) for three hours at 0°C followed by several washes with Holtfreter's. Samples were then postfixed with both 2% osmium tetroxide and 2% uranyl acetate for two and one hours, respectively, with several washes in between fixations. Oocytes were then dehydrated through a graded alcohol series, critical-point dried (Polaron dryer) in carbon dioxide, and mounted on stubs. Samples were then sputter-coated with gold (thickness approximately 6 nm) in a Polaron SEM coating unit and viewed at 5–10 kV.

Electrophysiology

Electrophysiology was performed at room temperature (22–25°C) in small plastic recording chambers filled with low Ca^{2+} Holtfreter's which contained: 59.93 mM NaCl, 0.67 mM KCl, 2.38 mM $NaHCO_3$, and 0.005 mM $CaCl_2{\cdot}2H_20$, pH = 7.8 (after Anderson et al., '94). Measurements of FEOs also utilized poly-lysine coated chambers (1:10 dilution of a 1% high molecular weight stock solution; Sigma P-1524, St. Louis, MO) to prevent rolling. Oocytes were positioned with their equatorial plane perpendicular to the dish, enabling measurements to be recorded from the animal and vegetal poles. The preparation was then placed on a platform situated over a camera-equipped microscope, allowing images to be visualized on a monitor. The ion specific electrode with DC amplifier (IP Amp, Ion Polarographic Amplifier, Applicable Electronics, Sandwich, MA) and ground electrode were then submersed into the experimental chamber. The entire assembly on a ¼ inch steel plate is located inside a Faraday cage suspended on air tubes over a ½ inch steel plate for vibration suppression.

The simultaneous collection of H^+ and K^+ (and H^+ and HCO_3^-) was performed with the dual-probe IP-Amp system using Automated Scanning Electrode Technique (ASET) software (Sciencewares, Falmouth, MA). H^+ and K^+ electrodes, located on separate preamplifier heads, were positioned approximately 60 μm apart as a fixed array during data collection using three orthogonal microscrews. To determine the distance between the two electrodes, two cameras were utilized providing

an overhead (XY) and a frontal view (XZ). In the grid scans performed, the two electrodes collected data from five different positions in the Z axis. Of these five positions 60 μm apart, only the three closest overlapping Z locations were utilized, with their averages being plotted against one another. This averaging method is one current approach adjusting for the 60 μm separation distance between the two measuring electrodes.

The manner in which the ion-selective electrodes collect data is as follows. The microelectrode steps 10 μm in an orthogonal pattern from an observation point close to the surface of the oocyte in order to measure X, Y, and Z components of the ionic flux. This sampling routine is performed three times before moving to the next point-of-interest. Data can be collected in "grids" of points-of-interest by programming the electrode to move over a desired distance in a chosen number of steps in the desired X, Y, and/or Z axes. These scans can vary from a few points in one axis to hundreds of points in all three axes. Ion movement can then be expressed in pmol/cm^2/sec using Fick's law (ion flux, J = –D dC/dr where D is the diffusion coefficient for the ion, dC is the concentration differential, and dr the spatial differential). Bicarbonate fluxes were then calculated from carbonate concentrations using the Henderson-Hasselbalch equation. The defined set of observation points is reached via micro stepper motors with submicron motion capabilities controlled by the ASET Software for Windows (developed by Eric Karplus of Sciencewares in Falmouth, MA). An analog to digital (A/D) board converts the digitizing electrode signal into potential differences, averaging 1,000 samples per second at each apex of the 10 μm orthogonal sampling path at a point-of-interest.

Ion-selective electrodes

Microelectrodes were pulled from glass capillary tubes (World Precision Instruments, Sarasota, FL; #TW 150-4 with 1.12 and 1.5 mm inner and outer diameters, respectively) using a Sutter P-97 Flaming Brown pipette puller. These electrodes, with a 2 μm tip diameter, were positioned about 5 μm from the surface of the oocyte at closest approach. The noninvasive proton selective electrode, NVP_H, back filled with 100 mM KCL/H_2PO_4 (pH 7.0) as the electrolyte, had a 15–25 μm column of liquid ion exchanger (LIX) cocktail front-filled in the tip (Fluka Hydrogen Ionophore I-cocktail B). Carbonate selective electrodes were backfilled with 10 mM $NaHCO_3$ in 150 mM NaCl, pH = 7.0, and frontfilled with a 20 μm column of LIX (WPI #IE-310). Potassium electrodes, backfilled with 100 mM KCl (pH = 7.0), were front filled with 180 μm of LIX (Fluka Potassium Ionophore I-cocktail B). Electrical contact was established with an Ag/AgCl wire inserted into the electrolyte. Return electrodes were either 3 M KCl or 3 M NaCl in 1% agarose (Sigma, A-6877).

Calibration of ion-selective electrodes

Prior to the collection of biological data, it was necessary to calibrate the ion-selective electrodes to determine the efficiency of each (which is dependent on several factors including the properties of the ionophore and the method of data acquisition). Ion concentrations, measured known distances from an artificial source containing the ion of interest, can be plotted against their distance from the source (Fig. 1A). An unknown parameter, the distance from the closest approach to the theoretical infinite source of ions, needed to be estimated. Subsequently, the plotting of the ion concentration versus inverse distance from the source results in a straight line demonstrating a linear relationship between these two variables (Fig. 1B). We can then use this assumed 100% efficient linear relationship using the static electrode to predict the μV difference measured by the dynamic electrode at the same distances from the source. These expected μV differences could then be compared to the observed μV values to determine the efficiency of the dynamic electrode (Fig. 1C).

To determine this efficiency, a calibration curve was constructed using the following equation:

$$dV = \frac{\text{eff} \bullet S \bullet K \bullet dr}{e \bullet z \bullet r^2 \bullet (Cb + K/(r + dr/2))} \quad \text{(mV)}$$

where Cb = background [ion], dr = oscillation distance, e = base of natural logarithms, eff = efficiency of the measure, K = slope of ion curve (obtained in Fig. 1B), r = distance to the point source, S = Nernst coefficient (29 and 58 mV for divalent and monovalent ions, respectively), and z = unit charge on the ion. Electrode efficiencies for H^+, K^+, and CO_3^{2-} were determined to be 63%, 85%, and 40%, respectively. Proton efficiency is particularly dependent on buffer concentration, and doubling of the buffer in the Holtfreter's Solution resulted in a reduction of the efficiency to 46% (unpublished results). As a result, slightly buffered Holtfreter's solution was utilized during proton data collection.

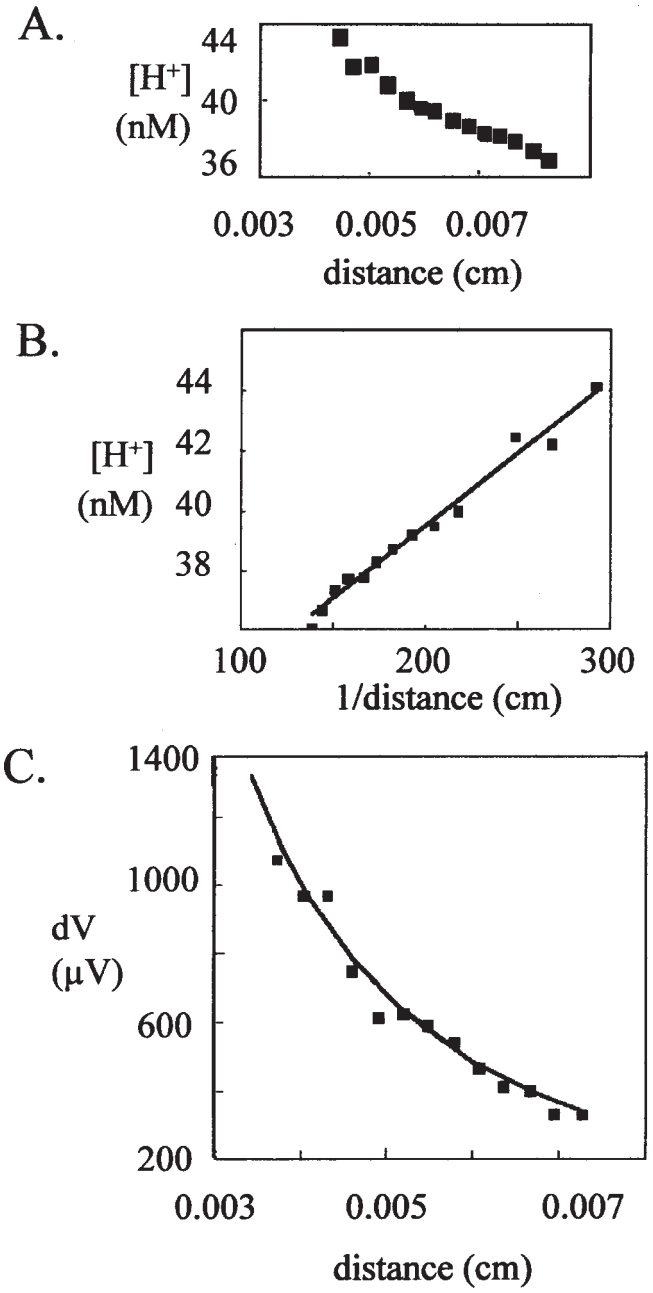

Fig. 1. Efficiency of H^+ electrode. To determine the efficiency of this electrode, H^+ ion concentrations were measured at known distances from an artificial source. Two plots were then constructed using this data: **A.** the measured concentration of H^+ ions (mV) vs. the distance from the source; **B.** the conversion of this hyperbola into a linear form by plotting the concentration of H^+ vs. 1/distance; and **C.** the actual and theoretical μV data used in determining the efficiency of the electrode (63%).

Silanization

In order to stabilize the short column lengths of the hydrophobic LIX cocktails, glass electrodes were silanized prior to use (hydroxyl groups on the glass surface condense with an unstable silanol). After being pulled, microelectrodes were dried overnight at 250°C. Microelectrodes were silanized in a one liter glass chamber for ten minutes by injecting 50 μl dimethyl chlorosilane (Sigma) into the chamber. After airing out the chamber, the microelectrodes were baked (covered) for 1–2 hours and stored at 180°C in a separate oven until use.

Pharmacology

ATPase pump inhibitors, ortho-vanadate and N-ethyl maleimide (NEM), S-6508 and E-3876, respectively, were obtained from Sigma (Macara et al., '80; Forgac et al. '83) and prepared according to Ehrenspeck ('80). The final concentrations of both inhibitors were 0.01 mM, 0.1 mM, and 1 mM (NEM only). Initial proton flux was recorded for 20–30 minutes, at which time, the normal low Ca^{2+} Holtfreter's solution was replaced with the inhibitor solution. After 20–30 minutes, the oocyte was returned to the original solution. Significance ($P < 0.05$) and reversibility of inhibition could then be determined.

Statistical analysis

Data were exported from the measurement software, ASET, into spreadsheets for appropriate calculations including the averages and medians of the three flux measurements in the X dimension, as well as those for the Y and Z dimensions, that were obtained at each observation point. By calculating and using the median of three measurements of X, Y and Z, rather than the mean, potential outlying data values were eliminated in situations that were physically or electrically noisy. This provided the advantages of using a measure of central tendency (mean or median) while also eliminating noise (which distorts a mean). Medians for each dimension could then be combined to display 3-D flux vectors. Analysis of the data was performed utilizing factorial design analysis of variance in which a matrix equation, $Y = X\beta$, describes an experiment. By creating an n by p design matrix, X, for each experiment, it was possible to examine the n by 1 data matrix (Y) for the significance of a p by 1 matrix of factors, β, within that experiment. This analytic approach allows us to examine multiple factors simultaneously, rather than one factor per experiment, and also allows the study of factor interactions that may be of interest in themselves.

In addition, the incorporation of orthogonal polynomials in the design matrix aids in the determi-

nation of the degree or type of curvilinearity of the data. For example, the data may have linear and quadratic components of response to certain factors, such as time or Z position, in which a steady increase/decrease occurs (linear) in combination with an irregular rise/decline (quadratic, quartic, etc.) due to the factor of interest. These tests were important in determining the stability of the recorded fluxes during data collection. The data and design matrices were analyzed with a factorial design multivariate analysis program, MULVAR, written by J.G. Kunkel in STSC APL (version 8.0) and currently available translated into the multiplatform language J. Tabular output from MULVAR allowed appropriate significance tests to be applied for specific factors and interactions in an experiment. Some regression and correlation analysis of the H^+ and K^+ data was performed with the statistical program, CRUNCH (Berkely, CA). Binomial pump inhibition and equatorial data were analyzed using Chi Square (χ^2) analysis.

RESULTS

Independent H^+, K^+, and HCO_3^- fluxes

All proton fluxes recorded were outward regardless of oocyte stage and presence/absence of follicular tissue. The 3-dimensional pattern of H^+ efflux from a *Xenopus* oocyte using ion-specific electrodes is shown in Fig. 2. Seven by seven grid scans (10 μm from the surface of the oocyte) were performed at the animal and vegetal hemispheres of a stage VI follicle-enclosed oocyte. From X, Y, and Z dimensional flux measurements over an area of 600 × 600 μm at 60 μm spacing, it was possible to display a stereo image of the flux vectors using the 3-dimensional graphic program, MAGE (Richardson and Richardson, '94). Implementation of grid scans not only provided visualization of flux patterns but they also provided temporal and spatial evidence that the fluxes being recorded were steady currents emanating from a broad source and not point sources resulting from possible injury to the oocyte.

Subsequent grid scans, performed over a 240 μm area at the animal and vegetal hemispheres, collected flux data over a 30 minute period. The results illustrate various H^+ flux patterns that are influenced by the developmental stage and hemisphere of the oocyte and the surrounding follicular tissue. While there are some interesting trends observed, the overwhelming impression is of a high degree of variability. Although oocytes were overall consistent within a grid area suggesting local stability of the currents, at different locations and at the various stages of development they do not demonstrate 100% consistency, making interpretation very difficult (data not shown).

K^+ and HCO_3^- fluxes were also recorded at the animal and vegetal hemispheres of stage V and VI oocytes with and without surrounding follicular tissue. Both influxes and effluxes of K^+ were measured; however, only effluxes of HCO_3^- were detected. Again, these fluxes, while consistent within a grid area, were seen to vary with the developmental stage of the oocyte and the presence of follicular tissue but the data exhibit a high degree of variability between individuals (data not shown).

Equatorial region

In addition to grid scans being performed at the two opposing poles, individual H^+ and K^+ data were also recorded at the equator. The direction and strength of these fluxes were analyzed with an F-test ($P < 0.05$) and χ^2. The presence/absence

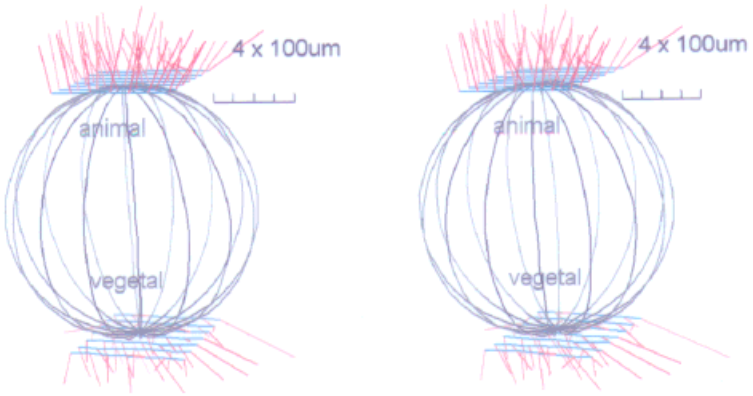

Fig. 2. Proton flux recorded from the animal and vegetal hemispheres of a stage VI FEO. A 7 × 7 grid scan was performed over a 600 μm × 600 μm approximately 10 μm from the surface of the oocyte.

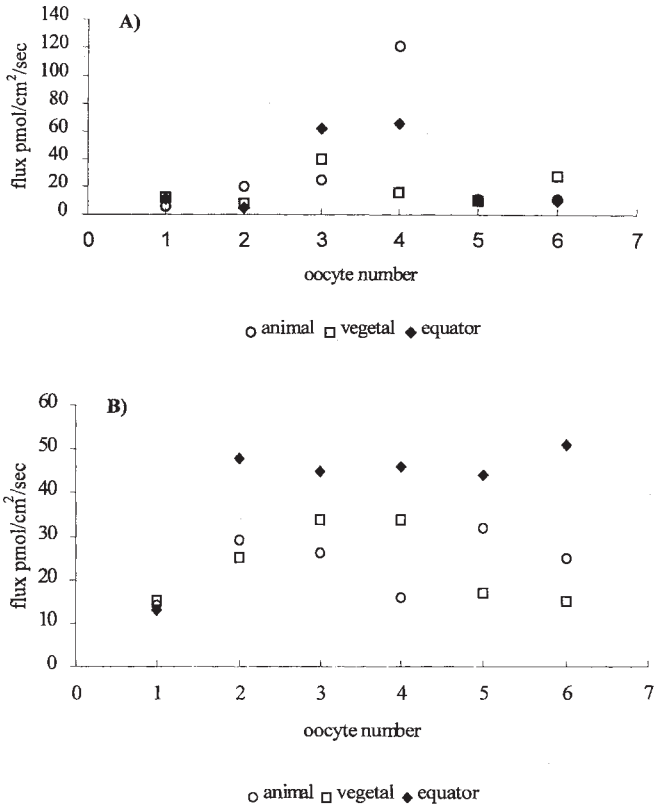

Fig. 3. Proton effluxes recorded from animal and vegetal hemispheres and equator in stage V (**A**) and stage VI (**B**) oocytes. Six oocytes from each stage were measured and the total flux in pmol/cm^2/sec was calculated.

of follicular tissue did not have any apparent affect on the distribution of H^+ fluxes; therefore, the oocytes were classified only according to stage of maturation (Fig. 3). In the six stage V oocytes measured, only one demonstrated a greater efflux at the equator than both the animal and vegetal hemispheres. The fluxes at both poles had varying strengths with no apparent trends. Stage VI, on the other hand, had the greatest flux at the equator in five of the six oocytes measured; however, subsequent χ^2 analysis resulted in no significant differences.

With regards to K^+ fluxes recorded at the equatorial region, only the direction and not the magnitude appeared to be influenced by the presence/absence of follicular tissue and not developmental stage (data not shown). As previously reported, we measured both influxes and effluxes with the direction being influenced by the presence/absence of follicular tissue and not developmental stage. In all defolliculated oocytes measured, equatorial fluxes were always traveling in the same direction as those at the vegetal pole. FEOs, however, displayed a different trend with K^+ fluxes traveling in the same direction as those recorded at the animal pole (and not the vegetal pole as seen in defolliculated oocytes).

Multiple simultaneous ion probes

To validate the usefulness of a multiple probe system, H^+ and CO_3^{2-} fluxes were measured from an artificial Na_2CO_3 point source using the dual probe IP-AMP system as previously described (Fig. 4). The observed H^+ gradient was more dispersed than its distinct CO_3^{2-} counterpart due to the rapid diffusion of H^+ ions as well as their known quenching by buffers. The two μV-gradient peaks that were recorded are approximately 60 μm apart due to the separation distance between the tips of the two electrode array.

Once this technique was validated, H^+ and K^+ data were simultaneously collected from the animal and vegetal hemispheres of stage VI defolliculated and FEOs (Fig. 5). In the four defolliculated oocytes measured, only positive fluxes (effluxes) were recorded with the H^+ electrode while both positive (effluxes) and negative (influxes) fluxes were measured with the K^+ electrode. At both hemispheres, large H^+ effluxes were accompanied by large K^+ influxes. Linear regression analyses of the data resulted in significant negative correlations between $H^+$and K^+ fluxes at the animal ($r^2 = 0.8774$; $P < 0.01$) and vegetal poles ($r^2 = 0.79$; $P < 0.02$). In the eight FEOs measured, again, effluxes of H^+ and influxes and effluxes of K^+ were

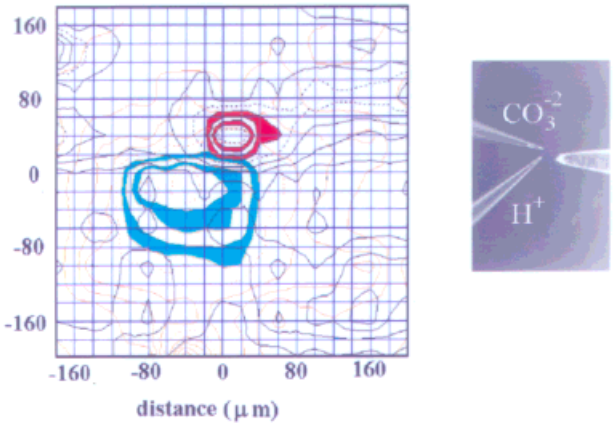

Fig. 4. Proton (gray) and carbonate (black) fluxes measured from a Na_2CO_3 source. Note: since the electrodes are approximately 60 μm apart, the peaks of the gradients appear to have different X and Y coordinates. Once this separation is accounted for, however, these two peaks are superimposed on one another. In addition, notice the distinct CO_3^{2-} plot versus its dispersed H^+ counterpart.

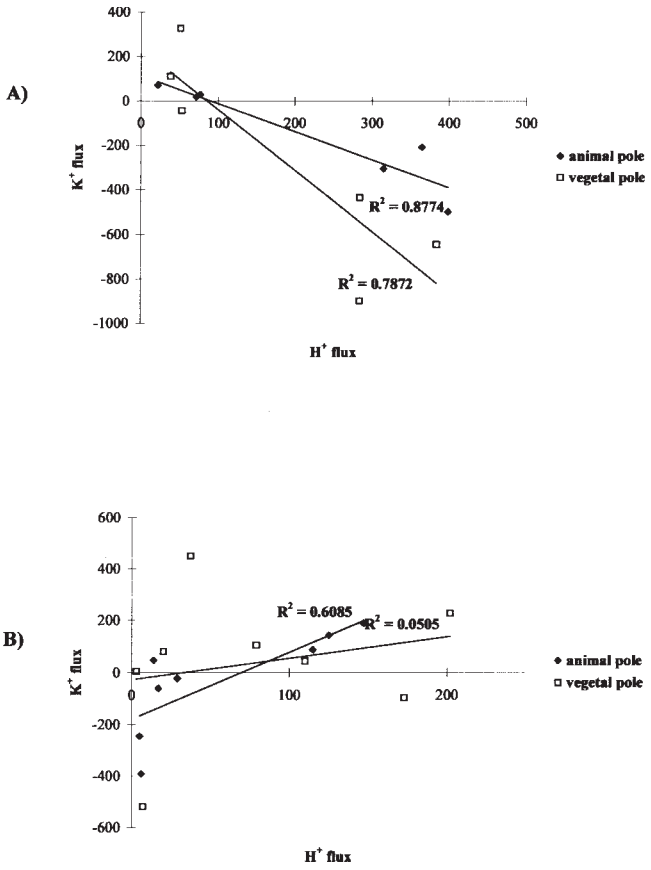

Fig. 5. Regression analysis of H^+ and K^+ data collected from stage VI defolliculated (**A**) and follicle-enclosed (**B**) *Xenopus* oocytes from animal (solid diamond) and vegetal (open square) poles. To study the possible relationships between H^+ and K^+ fluxes, H^+ and K^+ data were plotted along the horizontal and vertical axes. By using the method of least squares, a straight line was fitted to the data. This linear regression (calculation of r^2) can be used to predict the K^+ fluxes given the H^+ flux.

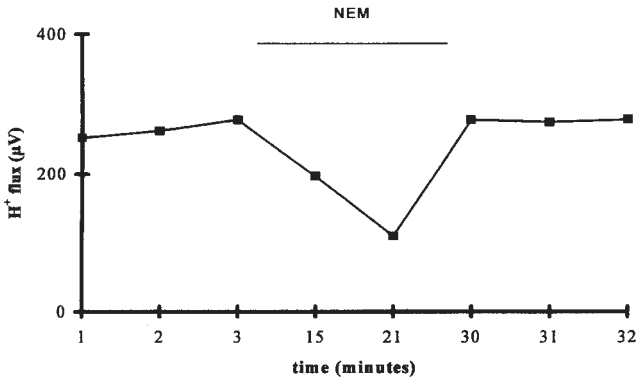

Fig. 6. The proton secretion from a FEO reversibly inhibited by 1 mM N-ethyl maleimide (a representative experiment is shown). Oocytes were immersed in low Ca^{2+}Holtfreter's (standard electrophysiological solution) and the flux was measured for 20–30 minutes. The oocyte was then perfused with the inhibitor solution (containing low Ca^{2+}Holtfreter's with a final concentration of 1mM NEM), data were collected for 20–30 minutes, and then the oocyte was returned to the initial medium for final recordings. Analysis of the data with an F-test ($P < 0.05$) showed the original H^+ flux to have a significant difference only when subjected to the inhibitor and not with the ending flux.

recorded. A significant positive correlation between these two ionic fluxes was seen only at the animal pole, in which large H^+ effluxes were accompanied by large K^+ effluxes ($r^2 = 0.6085$; $P < 0.02$). The H^+ and K^+ fluxes at the vegetal pole, although traveling in the same direction (outward), had no significant correlation ($r^2 = 0.05049$; $P = 0.77$).

Effect of pump inhibitors

Initial results indicated that 33% of all oocytes had a significant (reversible) decrease in H^+ flux with both NEM and vanadate (Fig. 6). Utilization of χ^2 tests, however, resulted in only one significant difference in the proportions among oocyte populations between 0.01mM NEM and 1.0mM NEM ($\chi^2 = 4.073$, df = 1). Based on these results, it is very difficult to derive conclusions regarding V and P type pumps (such as location) other than they do contribute to the observed H^+ flux when only paying attention to the one ion, protons.

DISCUSSION

In the present study, we have examined the flux distribution patterns of H^+, K^+, and HCO_3^- ions around developing *Xenopus* oocytes in an attempt to further characterize the asymmetric current initially described by Robinson ('79). In his use of the voltage probe, Robinson had calculated the net current of defolliculated oocytes as 10 nA (approximately 10 pmol/cm^2/sec); however, he could only suggest possible gross currents of ions that were responsible for adding up to this net current. Subsequent research using ion replacement and agonist/antagonist treatment has suggested that this net current is carried mainly by chloride ions; but little is known about the contribution of other ion types.

We have pursued this lack of information with ion-selective electrodes and discovered that hidden within that 10 pmol current, there are substantial pmol effluxes of H^+ and HCO_3^- and inward and outward fluxes of K^+ that vary with developmental stage. We have documented a direct correlation between H^+ and K^+ fluxes through the use of simultaneous multiple ion data collection. We have recorded substantial ion transport at the

equatorial region of the oocyte, which was previously thought to have little activity and, lastly, we have determined that any involvement of ATPase pumps in H^+ flow is not directly correlated to the presence of follicular tissue.

The involvement of H^+ and K^+ fluxes in development as indicated by our results support the findings of prior ion transport studies. For example, the involvement of H^+ gradients in solute transport (Beers et al., '82), protein transport (Schatz and Butow, '83), and vitellogenin uptake (Stynen et al., '88) has been established. The H^+ pump current has also been linked to aerobic metabolism in that low pH inhibits glycolysis and the synthesis of protein, RNA, and DNA (Ehrenfield et al., '85; Restrepo et al., '90; Sater et al., '94). Our results indicated a greater H^+ efflux at the animal pole of the oocyte. The germinal vesicle is located in this hemisphere and its high metabolic activity may account for the observed greater H^+ efflux. In addition, the influence of developmental stage on H^+ flux (and hence, intracellular pH) as demonstrated by our research correlates with prior research. Cytoplasmic alkalinization in *Xenopus* oocytes, which occurs during maturation (Chambard and Pousysségar, '86), is followed by acidification in the *Xenopus* embryo, leading to posterior axis formation (Gutknecht et al., '95).

The involvement of HCO_3^- in pH_i regulation has been established (Wietasch and Kraig, '91). For example, the role of the HCO_3^-/Cl^- exchanger as an alkali extruder has been documented in several mammalian studies (Alper, '94; Zhao and Baltz, '96). Two types of cotransporters, K^+/HCO_3^- and Na^+/HCO_3^-, have also been identified in squid axons and salamander kidneys, respectively, and function in the same role (Zhao et al., '95; Boron et al., '97). The participation of HCO_3^- in pH_i regulation may also be supported by this research; however, HCO_3^- fluxes were minimal (compared to H^+ fluxes) and therefore, the results are perhaps not of practical significance from a buffer perspective.

The involvement of K^+ ions in early development, however, is still unclear. Research with K^+channel agonists has suggested that this ion plays a role in meiosis with the promotion of germinal vesicle breakdown (Honoré and Lazdunski, '93; Wilbrand et al., '93). Furthermore, receptors located on the follicle cell layer (implicated in the generation of the K^+ current) have also been suggested to play a role in the maturation process at ovulation (King et al., '96). Our results demonstrating an increase in K^+ flux with developmental stage support these hypotheses.

Our research has also demonstrated the informational power of collecting simultaneous multiple ion data. The individual H^+ and K^+ data, although they show some interesting characteristics, are very difficult to interpret independently of one another. Use of a multi-probe array, however, has allowed for the direct study of the correlation and directionality of these fluxes and has helped explain the observed variability when they were examined singly. This correlation helps explain the confusing reversals of flux patterns of K^+ that were observed in specific oocytes, which are now understood to be correlated with H^+ flux. These correlations would also prove useful when conducting experiments with limited sample sizes since there are observed variability among oocyte populations regardless of the sample size. This use of covariate probe measurements could reduce observed variability due to age of frogs (King et al., '96), variations in pump structure due to the presence of different isoforms (Chatterjee et al., '92), or the utilization of different donor frogs. The donor frog effect results in a response pattern similarity in all the oocytes of the same frog but a substantially different response among oocytes from different frogs (Lotan et al., '86; King et al., '96). Therefore, experiments with limited sample sizes would still prove useful when collecting simultaneous ion probe measurements.

The close relationship between K^+ and H^+ fluxes that we have documented using this new technique has also been reported in prior studies on other tissues. Potassium channel regulation by pH (an increase in K^+ channel activity with cytoplasmic alkalinization) has been documented in amphibian distal tubules (Cooper and Hunter, '97). Alternately, acidification has been shown to reduce the transmembrane K^+ flux in kidney tubules (Tsai et al., '95) and the cAMP-activated K^+ current in *Xenopus* oocytes by decreasing gap junctional conductance (Greenfield et al., '90). Our observation of a negative correlation between H^+ and K^+ fluxes in defolliculated oocytes (with large H^+ effluxes accompanied by large K^+ influxes) may be a direct result of this regulation of K^+ channels by pH or possibly the control of membrane potential.

We also examined ion flux at the equatorial region of the oocyte and inhibition of H^+ flux with ATPase pump inhibitors. In these experiments, individual ion fluxes were measured and subsequent statistical analysis of the data resulted in

essentially no apparent trends (the only significant difference we observed was between the highest and lowest concentration of NEM in the pump inhibition experiments). If multiple ion fluxes were recorded during these experiments, however, we could have accounted for variability with the correlation between fluxes. Since we did not discover this correlation until later, however, we could not account for this variability, again demonstrating the importance of covariance analysis in ion probe studies.

Our identification of H^+, K^+, and HCO_3^- fluxes around developing *Xenopus* oocytes with dynamic ion-selective electrodes has enabled us to contribute to the initial electrophysiological work by Robinson ('79). We have described how these fluxes are dependent on the developmental stage of the oocyte and to some degree, ATPase pumps. We have also documented a direct correlation between ion fluxes demonstrating the need for the simultaneous data collection of multiple ion types.

Utilization of this technique has also resulted in the ability to collect 3-dimensional data at any point around a developing oocyte for an extended period of time. The recorded data have both directionality and strength, allowing for better visualization of individual ion fluxes and their physical origins. With the newly acquired 3-dimensionality of data, we are then able to construct an observed flux gradient pattern around a fully matured oocyte (Fig. 7). We can use this information of flux direction and magnitude to start understanding the complexity that underlies the net current. Individual fluxes of additional ion types such as Na^+, Ca^{2+}, and Cl^-, must also be examined and included in the computation of net flux. The resulting combination of influxes and effluxes could then be tabulated and compared to the asymmetric currents in fucoid eggs, insect and amphibian oocytes, and mammalian systems. This physiological approach to early development may provide information to correlate the observed phenomenon of polarity determination with a set of ionic fluxes driving or resulting from biochemistry and physiology of the egg.

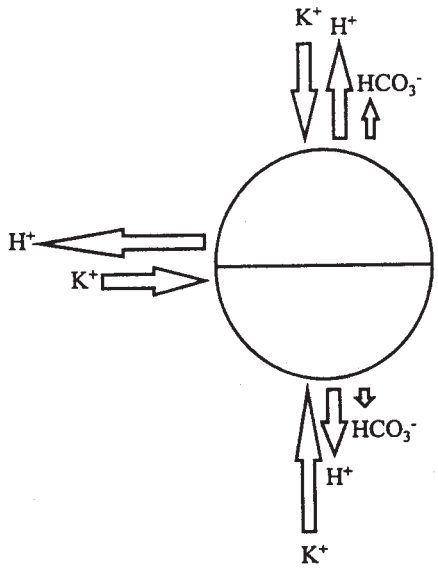

Fig. 7. Schematic diagram illustrating the flux pattern of a defolliculated *Xenopus* oocyte (diameter 1.2 mm). The length of the arrow is representative of the magnitude of fluxes.

ACKNOWLEDGMENTS

The authors thank Al Shipley for his technical support of the electronics, and Eric Karplus for his creative writing of the software. Terena Holdeway-Clarke provided helpful discussions of the manuscript. Financial support for this project and EEF was provided by Applicable Electronics of Forestdale, Massachusetts.

LITERATURE CITED

Alper SL. 1994. The band 3-related anion exchanger (AE) gene family. Cell Physiol Biochem 4:265–281.

Anderson M, Bowdan E, Kunkel JG. 1994. Comparison of defolliculated oocytes and intact follicles of the cockroach using the vibrating probe to record steady currents. Dev Biol 162:111–122.

Barish ME. 1983. A transient calcium-dependent chloride current in the immature *Xenopus* oocyte. J Physiol (Lond) 342:309–325.

Beers MF, Cart SE, Johnson RG, Scarpa A. 1982. H^+-ATPase and catecholamine transport in chromaffin granules. Ann NY Acad Sci 402:116–133.

Boron WF, Hediger MA, Boulpaep EL, Romero MF. 1997. The renal electrogenic Na^+:HCO_3^- cotransporter. J Exp Biol 200:263–268.

Bowdan E, Kunkel JG. 1990. Ionic components of dorsal and ventral currents in vitellogenic follicles of the cockroach, *Blatella germanica*. J Insect Physiol 40(4):323–331.

Chambard J-C, Pouyssegur J. 1986. Intracellular pH controls growth factor-induced ribosomal protein S6 phosphorylation and protein synthesis in the G0-G1 transition of fibroblasts. Exp Cell Res 164:282–294.

Chatterjee D, Charkraborty M, Leit M, Neff L, Jamsa-Kellokumpu S, Fuchs R, Baron R. 1992. Sensitivity to vanadate and isoforms of subunits A and B distinguish the osteoclast proton pump from other vacuolar H^+ ATPases. Proc Natl Acad Sci USA 89:6257–6261.

Cooper GJ, Hunter M. 1997. Intracellular pH and calcium in frog early distal tubule: effects of transport inhibitors. J Physiol (Lond) 498:49–59.

Dröse S, Altendorf K. 1997. Bafilomycins and concanamycins as inhibitors of V-ATPases and P-ATPases. J Exp Biol 200:1–8.

Dumont JN. 1972. Oogenesis in *Xenopus laevis* (Daudin). I. Stages of oocyte development in laboratory maintained animals. J Morphol 136:153–180.

Ehrenfield J, Garcia-Romeu F, Harvey B. 1985. Electrogenic active proton pump in *Rana esculenta* skin and its role in sodium ion transport. J Physiol (Lond) 359:331–355.

Ehrenspeck G. 1980. Vanadate induced inhibition of sodium transport and sodium dependent anion transport in turtle bladder. Biochem Biophys Acta 601:427–432.

Etheridge AL, Richter MA. 1978. *Xenopus laevis*, rearing and breeding the African clawed frog. Nasco, WI: p 3–4.

Forgac M, Cantley L, Wiedenmann B, Altstiel L, Branton D. 1983. Clathrin-coated vesicles contain an ATP-independent proton pump. Proc Natl Acad Sci USA 80:1300–1303.

Greenfield LJ, Hackett JT, Linden J. 1990. *Xenopus* oocyte K^+ current. II Adenylyl cyclase-linked receptors on follicle cells. Am J Physiol 259:C784–C791.

Gutknecht DR, Koster CH, Tertoolen LGJ, de Laat SW, Durston AJ. 1995. Intracellular acidification of gastrula ectoderm is important for posterior axial development in *Xenopus*. Development 121:1911–1925.

Honoré E, Lazdunski M. 1993. Single-channel properties and regulation of pinacidil/glibenclamide-sensitive K^+ channels in follicular cells from *Xenopus* oocyte. Pflügers Arch 424:113–121.

Jaffe LF. 1966. Electrical currents through the developing *Fucus* egg. PNAS 56:1102–1109.

Jaffe LF, Levy S. 1987. Calcium gradients measured with a vibrating calcium-selective electrode. Proc 9th Ann Conf IEEE 9:779–781.

King BF, Wang S, Burnstock G. 1996. P_2 purinoceptor-activated inward currents in follicular oocytes of *Xenopus laevis*. J Physiol (Lond) 494(1):17–28.

Kunkel JG. 1986. Dorsoventral currents are associated with vitellogenesis in cockroach ovarioles. In: Nuccitelli R, editor. Ion current in development. New York: A.R. Liss. p 165–172.

Lotan I, Dascal N, Cohen S, Lass Y. 1986. ATP-evoked membrane responses in *Xenopus* oocytes. Pflügers Arch 406:158–162.

Macara IG, Kustin K, Cantley Jr, LC. 1980. Glutathione reduces cytoplasmic vanadate: mechanisms and physiological implications. Biochem Biophys Acta 629(1):95–106.

Miledi R. 1982. A calcium-dependent transient outward current in *Xenopus laevis* oocytes. Proc R Soc Lond B Biol Sci 215:491–497.

Miledi R, Woodward R. 1989. The effect of defolliculation on the membrane current responses of *Xenopus* oocytes. J Physiol (Lond) 416:601–621.

Overall R, Jaffe LF. 1985. Patterns of ionic current through *Drosophila* follicles and eggs. Dev Biol 108:102–119.

Restrepo D, Cho DS, Kron MJ. 1990. Essential activation of Na^+-H^+ exchange by $[H^+]_i$ in HL-60 cells. Am J Physiol 259:C490–C502.

Richardson DC, Richardson JS. 1994. Kinemages— simple macromolecular graphics for interactive teaching and publication. Trends Biochem Sci 19:135–138.

Robinson KR. 1979. Electrical currents through full grown and maturing *Xenopus* oocytes. PNAS 76:837–841.

Rugh R. 1962. Experimental embryology: techniques and problems. Minneapolis: Burgess Pub. Co.

Sater AK, Alderton JM, Steinhardt RA. 1994. An increase in intracellular pH during neural induction in *Xenopus*. Development 120:433–442.

Schatz G, Butow RA. 1983. How are proteins imported into mitochondria? Cell 32:316–318.

Smith PJS, Sanger RH, Jaffe LF. 1994. The vibrating Ca^{2+} electrode: a new technique for detecting plasma membrane regions of Ca^{2+} influx and efflux. Methods Cell Biol 40:115–134.

Stynen D, Woodruff RI, Telfer WH. 1988. Effects of ionophores on vitellogenin uptake by Hyalophora oocytes. Arch Insect Biochem Physiol 8:261–276.

Tsai TD, Shuck ME, Thompson DP, Bienkowski MJ, Lee KS. 1995. Intracellular H^+ inhibits a cloned rat kidney outer medulla K^+ channel expressed in *Xenopus* oocytes. Am J Physiol 363:C1173–C1178.

Wietasch K, Kraig RP. 1991. Carbonic acid buffer species measured in real time with an intracellular microelectrode array. Am J Physiol 261:R760–R765.

Wilbrand F, Honoré E, Lazdunski M. 1993. Opening of glibenclamide-sensitive K^+ channel in follicular cells promote *Xenopus* oocyte maturation. Proc Natl Acad Sci USA 89:5133–5137.

Zhao Y, Baltz JM. 1996. Bicarbonate/chloride exchange and intracellular pH throughout preimplantation mouse embryo development. Am J Physiol 271:C1512–C1520.

Zhao Y, Chauvet PJP, Alper SL, Baltz JM. 1995. Expression and function of bicarbonate/chloride exchangers in the preimplantation mouse embryo. J Biol Chem 270:24428–24434.